DOI: 10.1002/chem.200902478

BCN: A Graphene Analogue with Remarkable Adsorptive Properties

Kalyan Raidongia,[a] Angshuman Nag,[a, b] K. P. S. S. Hembram,[a] Umesh V. Waghmare,[a] Ranjan Datta,[a] and C. N. R. Rao*[a, b]

Abstract: A new analogue of graphene containing boron, carbon and nitrogen (BCN) has been obtained by the reaction of high-surface-area activated charcoal with a mixture of boric acid and urea at 900 °C. X-ray photoelectron spectroscopy and electron energy-loss spectroscopy reveal the composition to be close to BCN. The X-ray diffraction pattern, high-resolution electron microscopy images and Raman spectrum indicate the presence of graphite-type layers with low sheet-to-sheet registry. Atomic force microscopy reveals the sample to consist of two to three layers of BCN, as in a few-layer graphene. BCN exhibits more electrical resistivity than graphene, but weaker magnetic features. BCN exhibits a surface area of 2911 $m^2 g^{-1}$, which is the highest value known for a $B_xC_yN_z$ composition. It exhibits high propensity for adsorbing CO_2 ($\approx$100 wt%) at 195 K and a hydrogen uptake of 2.6 wt% at 77 K. A first-principles pseudopotential-based DFT study shows the stable structure to consist of BN_3 and NB_3 motifs. The calculations also suggest the strongest CO_2 adsorption to occur with a binding energy of 3.7 kJ mol^{-1} compared with 2.0 kJ mol^{-1} on graphene.

Keywords: adsorption · BCN · desorption · graphene · materials science

Introduction

Analogues of graphite, containing boron, carbon and nitrogen (BCN) have attracted interest for some years and there has been some success in preparing $B_xC_yN_z$ compositions.[1] The subject has become of great interest recently because of the relevance of such materials to graphene, which is a two-dimensional network of sp^2-hybridised carbon atoms.[2–4] There are several reports in the literature of $B_xC_yN_z$ nanotubes of various compositions.[5–14] Nanotubes as well as bulk samples of BC_4N have been prepared by the reaction of B_2O_3, urea and carbon at high temperatures.[15,16] A material with the stoichiometry of BCN would be of particular interest because of its unique composition and possible interesting properties. It would indeed be instructive to compare the properties of BCN with those of graphite or graphene. Bartlett and co-workers[17] seem to have prepared a composition close to BCN by the reaction of BCl_3, NH_3 and acetylene. However, this sample could not be adequately characterised for its structure and properties. A composition close to BCN has been reported by reaction of the mesoporous carbon with B_2O_3 and N_2,[18] but the only property reported was its surface area. We, therefore, sought to prepare BCN by the reaction of a mixture of B_2O_3 and urea with activated charcoal of high surface area. This strategy was employed because of the reaction of low-surface-area carbon with urea and boric acid yields BC_4N. In this procedure, urea is used as a source of NH_3; a strategy that has been successful for the preparation of metal nitrides and oxynitrides.[19] Herein, we report the successful synthesis of a layered material composed of BCN with a high surface area and a great propensity for CO_2 uptake. Interestingly, the as-prepared material consists of only a few layers, as in graphene. We also report the results of first-principles DFT calculations[20–22] on BCN, which shed light on the structure and properties of this interesting material.

[a] K. Raidongia, Dr. A. Nag, Dr. K. P. S. S. Hembram, Prof. Dr. U. V. Waghmare, Dr. R. Datta, Prof. Dr. C. N. R. Rao
Chemistry and Physics of Materials Unit
International Centre for Materials Science
Theoretical Sciences Unit and
CSIR Centre of Excellence in Chemistry, Jawaharlal Nehru Centre for Advanced Scientific Research
Jakkur P.O., Bangalore 560064 (India)
Fax; (+91) 802-208-2760
E-mail: cnrrao@jncasr.ac.in

[b] Dr. A. Nag, Prof. Dr. C. N. R. Rao
Solid State and Structural Chemistry Unit
Indian Institute of Science, Bangalore 560012 (India)

Results and Discussion

Activated charcoal with a high surface area ($1256\,m^2g^{-1}$) constitutes the primary starting material for the synthesis of $B_xC_yN_z$ carried out by us. Reaction of the activated charcoal with urea and boric acid at 900 °C gave a product containing boron, carbon and nitrogen. The material obtained was soft and flaky. TEM investigations reveal a flake-like morphology. The TEM image in Figure 1 a shows the presence of

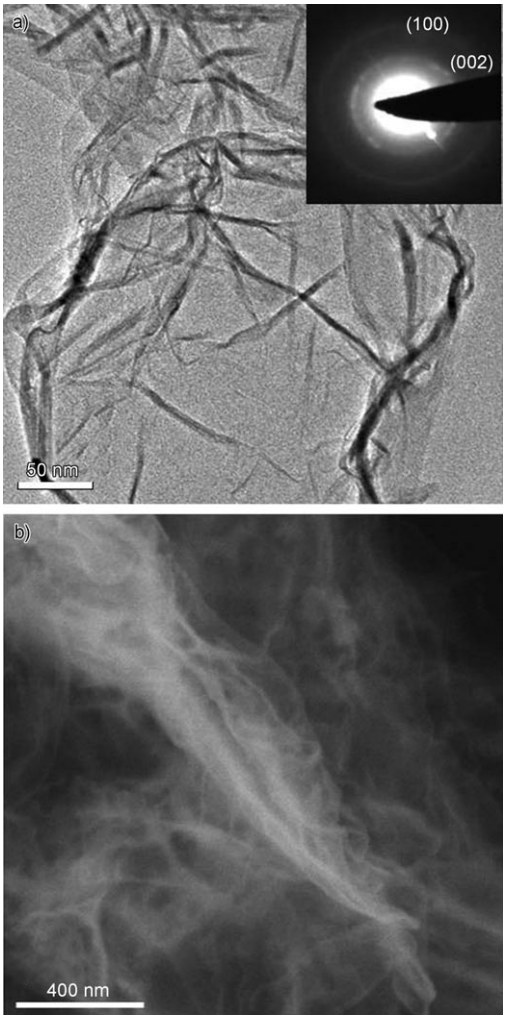

Figure 1. a) TEM image and b) FESEM image of BCN. Inset to a) is the corresponding selected-area electron diffraction (SAED) pattern.

BCN layers similar to few-layer graphenes.[3,23] The inset to Figure 1 a shows a selected-area electron diffraction (SAED) pattern with two rings due to the (002) and (100) reflections of the graphite-like material. The low-magnification FESEM image shows rippled and entangled nanosheets (Figure 1 b). The flakes are transparent and stable under the electron beam.

X-ray photoelectron spectroscopy (XPS) core-level spectra of the $B_xC_yN_z$ product are shown in Figure 2. The C 1s signal can be deconvoluted into bands at 283.1, 285.4 and

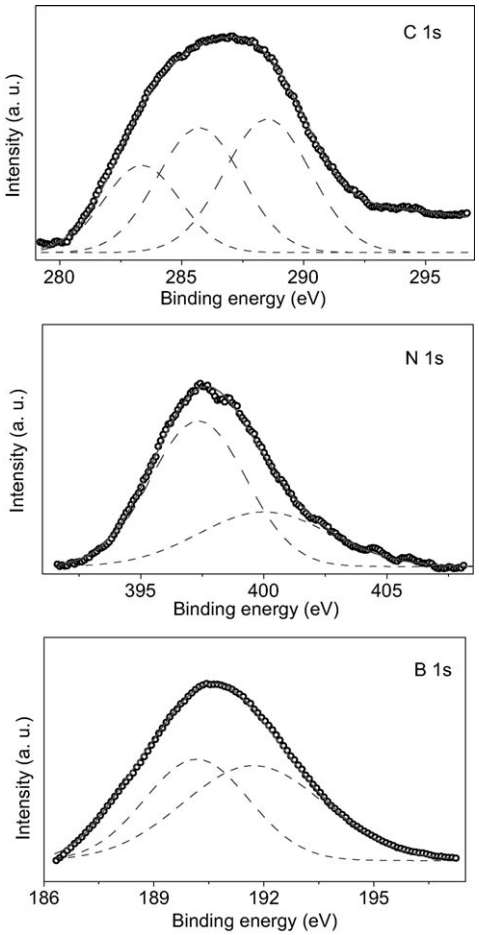

Figure 2. XPS data showing the core-level spectra (open squares) for C 1s, N 1s and B 1s for the BCN Sample. The dashed lines represent the deconvoluted component spectra.

288.2 eV, assigned to three different kinds of carbon atoms, bonded to boron, carbon and nitrogen respectively.[13] The N 1s signal can be deconvoluted into two bands at 397.1 and 399.8 eV. The former corresponds to nitrogen bonded to boron and the latter to nitrogen bonded to carbon.[13] The B 1s signal can be deconvoluted into two bands, of which the first one corresponds to boron bonded to carbon and second one is assigned to a boron atom bonded to nitrogen. Based on the capture cross sections and intensities of the B, C and N signals of the XPS core-level spectra, we estimated the composition to be $BC_{1.5}N_{1.1}$. To establish the elemental composition, we carried out electron energy-loss spectroscopy (EELS) measurements on the K-edge absorption for B, C and N in a high-resolution electron microscope. The EEL spectrum of the sample in Figure 3 a clearly shows the K-shell ionisation edges at $\approx$190, 284 and 401 eV for B, C and N, respectively. The two peaks at each core-edge fine structure is characteristic of the sp^2-hybridisation state, corresponding to π^* and σ^* bands, respectively, thereby indicating the graphite-like layered structure of the sample.[13] EELS measurements show the average chemical composi-

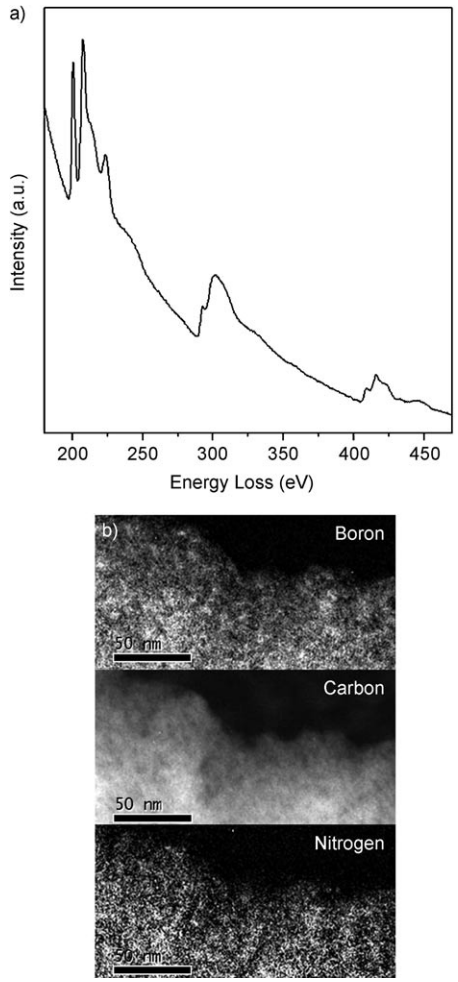

Figure 3. a) EEL spectrum and b) corresponding EEL map of boron, carbon and nitrogen of BCN (from TITAN microscope).

tion to be $BC_{1.2}N$. This analysis is in reasonable agreement with the analysis of XPS. For the purpose of convenience, we have approximated the composition to be BCN. The images in Figure 3b show elemental mapping of boron, carbon and nitrogen in a BCN flake. All three components are uniformly distributed throughout the flake, which confirms the homogeneous nature of BCN.

The XRD pattern of BCN, shown in the Figure 4a, is similar to patterns reported for graphitic materials with little sheet-to-sheet registry.[24,25] The pattern has two broad reflections with d spacings of 3.46 and 2.12 Å corresponding to the (002) and (100) planes, respectively. The interlayer distance in BCN (3.46 Å) is larger than that in graphite (3.33 Å) and hexagonal BN (3.36 Å). The Raman spectrum of BCN recorded with the 633 nm line from a HeNe laser is shown in Figure 4b. The spectrum is similar to that of graphitic materials with a D band at 1324 cm^{-1} and a G band at 1592 cm^{-1}.[3,26,27] The band at 2600 cm^{-1} may be due to a D+G combination band or a 2D overtone. The high-resolution TEM images (Figure 4c) mainly show 2 or 3 layers of BCN with an interplanar distance of 3.43 Å.

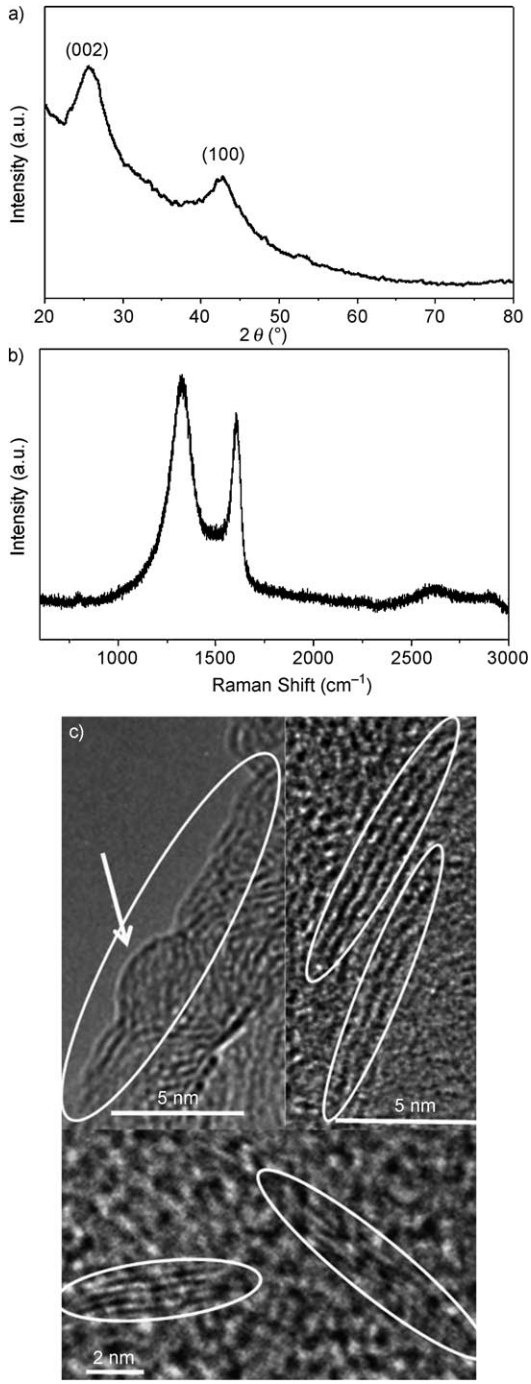

Figure 4. a) XRD pattern, b) Raman spectrum and c) high-resolution TEM image of BCN.

The basic reactions involved in the formation of BCN are the dehydration of $B(OH)_3$ and decomposition of urea, as shown in Equations (1) and (2):

$$2\,B(OH)_3 \xrightarrow{\Delta} B_2O_3 + 3\,H_2O \quad (1)$$

$$CO(NH_2)_2 \xrightarrow{\Delta} NH_3 + HNCO \quad (2)$$

The stoichiometric reaction for the formation of BCN may be written as shown in Equation (3):

$$B_2O_3 + 2\,NH_3 + 2\,C \xrightarrow{\Delta} 2\,BCN + 3\,H_2O \quad (3)$$

The overall reaction involves the release of gaseous species that could cause exfoliation and promote the incorporation of boron and nitrogen into the graphitic layers.

Thermogravimetric analysis curves of BCN and activated charcoal, carried out in air, are shown in Figure 5. BCN

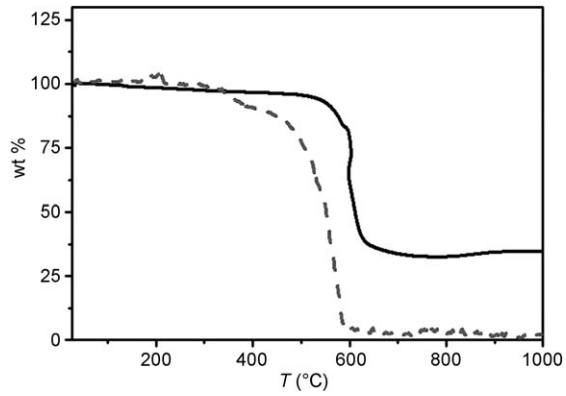

Figure 5. TGA curve of BCN (——) and activated charcoal (-----).

shows about 57% of weight loss at ≈600°C, leaving a residue that is stable up to 1000°C, whereas activated charcoal completely oxidises before 600°C. The XRD pattern of the residue in the case of BCN shows the presence of BN and C_3N_4. The approximate reaction of BCN in air can be written as shown in Equation (4):

$$12\,BCN + 15\,O_2 \rightarrow 4\,BN + C_3N_4 + 9\,CO_2 + 2\,N_2 + 4\,B_2O_3 \quad (4)$$

Figure 6 shows AFM images of BCN with the corresponding height profiles. The images show the thickness of the samples to be 1.1 and 0.65 nm, which corresponds to two and three layers, respectively. We find that the majority of BCN flakes possess two to three layers, with the occasional presence of single layers, as shown by the bar chart in Figure 6c. Thus, the AFM results clearly demonstrate that the BCN synthesised by us possessed only a few layers, resembling few-layer graphene rather than a graphitic material.

In Figure 7, we have compared the resistivity versus temperature plot of BCN with that of two to three layer graphene prepared by arc discharge of graphite in hydrogen.[28] Both show semiconducting behaviour, but BCN exhibits two orders of magnitude higher resistance than graphene.

We have examined the magnetic properties of BCN and the temperature-dependent magnetic properties at 500 Oe are shown in Figure 8. The data show divergence between field-cooled (FC) and zero-field-cooled (ZFC) data below 300 K. The divergence disappears at higher fields and the behaviour is somewhat similar to magnetically frustrated systems or phase-separated oxides. The Curie–Weiss temperature is −350 K, which shows antiferromagnetic interaction. However, the material shows a ferromagnetic hysteresis loop at 300 K, as shown in the inset of Figure 8. The values of saturation magnetisation and remnant magnetism are both very low and the coercive field is ≈175 Oe. Magnetism in BCN could arise from the contribution of edge effects and defects. The presence of both ferromagnetic and antiferromagnetic interactions in BCN are similar to graphene,[29] but the magnitude of the magnetic features is smaller in BCN.

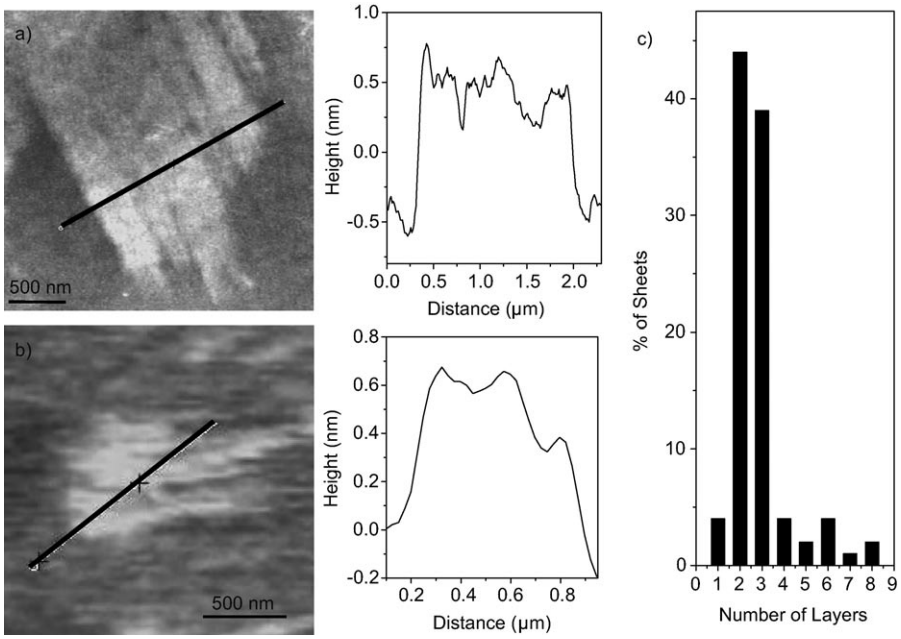

Figure 6. AFM images and corresponding height profile of a) two- and b) three-layered BCN. c) A bar chart showing the layer distribution of the BCN.

The nitrogen adsorption–desorption isotherm of BCN at 77 K is typical of a type I isotherm (Figure 9), which is characteristic of microporous materials.[30] With a small hysteresis loop, the isotherm is concave to the p/p_0 axis and the adsorption approaches a limiting value as $p/p_0 \rightarrow 1$. The surface area of BCN obtained by the BET method was 2911 $m^2 g^{-1}$. The pore size distribution, calculated from the adsorption isotherm, shows that the major contribution to the surface area is from the micropores (0.81 and 1.1 nm) with a small contribution from mesopores (2.5 nm), as can be seen from the inset in Figure 9. The sur-

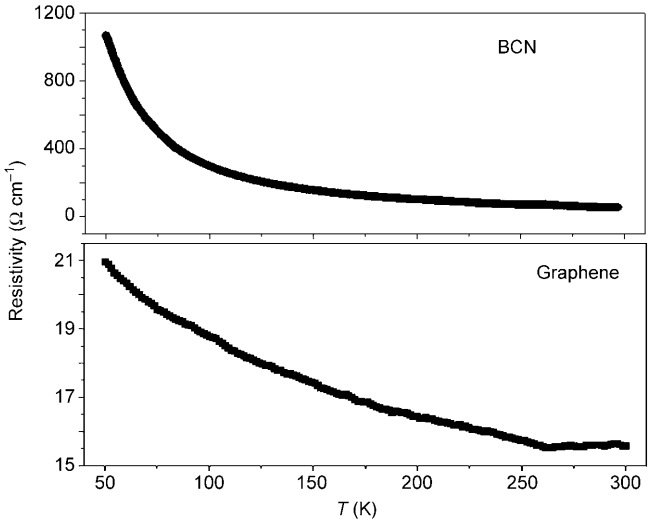

Figure 7. Resistivity of BCN and 2/3 layers of graphene, as a function of temperature.

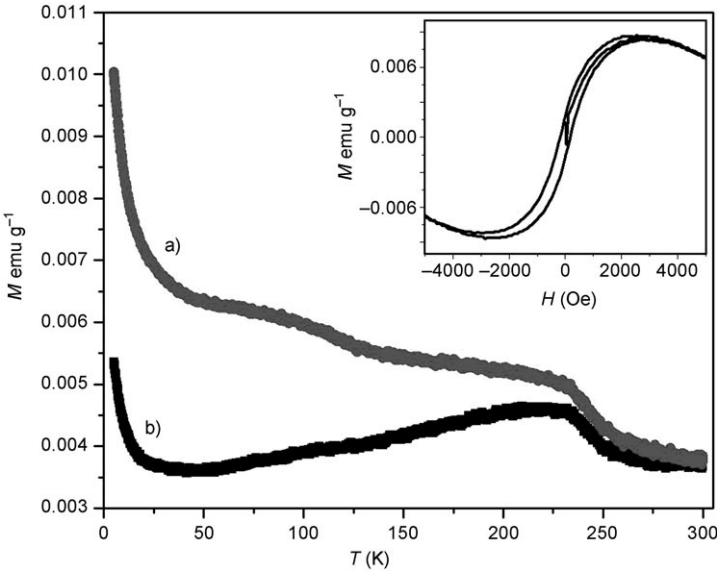

Figure 8. Temperature variation of magnetisation of BCN at 500 Oe showing the FC (a) and ZFC (b) data. The inset shows the magnetic hysteresis at 300 K.

face area of BCN is higher than any composition of the $B_xC_yN_z$ materials reported to date. The surface area obtained by us is four times higher than that reported for mesoporous BCN.[18] The high surface area of BCN prepared by us is consistent with the AFM observations that the material consists of two to three layers. It is known that the surface area of graphene increases with decreasing the number of layers. Graphene with two to three layers exhibits a surface area in the range of 1000 to 1800 m^2g^{-1},[31] which is somewhat lower than that of BCN.

Materials with good H_2 uptake have potential as clean-energy alternatives. We have examined H_2 adsorption on BCN at 77 K and 1 atm and found an uptake of 2.6 wt%.

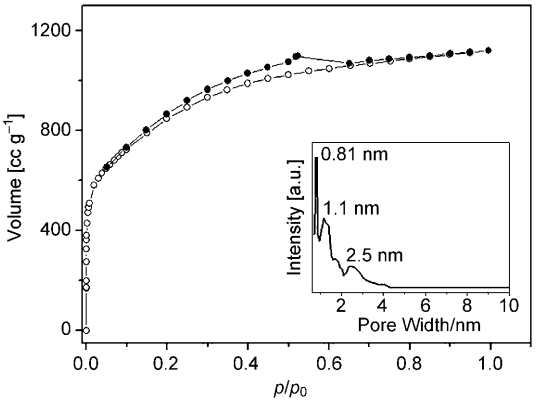

Figure 9. Nitrogen adsorption (○)–desorption (●) isotherms of BCN. The inset shows the pore size distribution of BCN.

Both adsorption and desorption isotherms of H_2 follow the same path, as shown in Figure 10a. H_2 uptake on BCN does not increase with increasing pressure. In Figure 10b, we show adsorption–desorption isotherms of H_2 on BCN carried out at 77 K and 50 bar. The adsorption isotherm rises sharply and reaches saturation at 10 bar, with 2.6 wt% H_2 uptake.

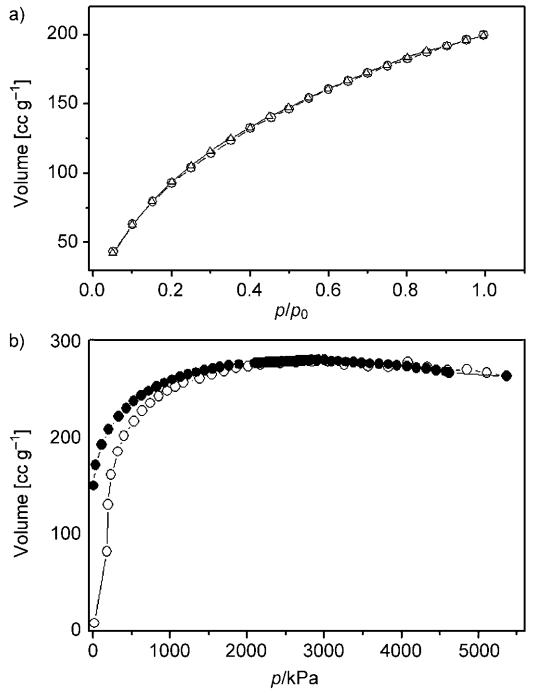

Figure 10. H_2 adsorption–desorption isotherms of BCN at a) 77 K and 1 atm (○: adsorption, △: desorption), b) 77 K and 55 bar (○: adsorption, ●: desorption).

Materials with good CO_2 adsorption capacity are of importance from both environmental and industrial points of view. BCN shows remarkably high CO_2 uptake of 100 wt% at 195 K and 1 atm, compared with 58% by the activated charcoal (starting material) under identical conditions. Ad-

sorption–desorption isotherms of CO_2 on BCN follow exactly the same path and do not reach saturation at $p/p_0 = 1$ (Figure 11a). However, at room temperature and 40 bar, the CO_2 uptake is 44 wt%, as shown in Figure 11b. The uptake of methanol vapour by BCN is about 26 wt% at room temperature and atmospheric pressure.

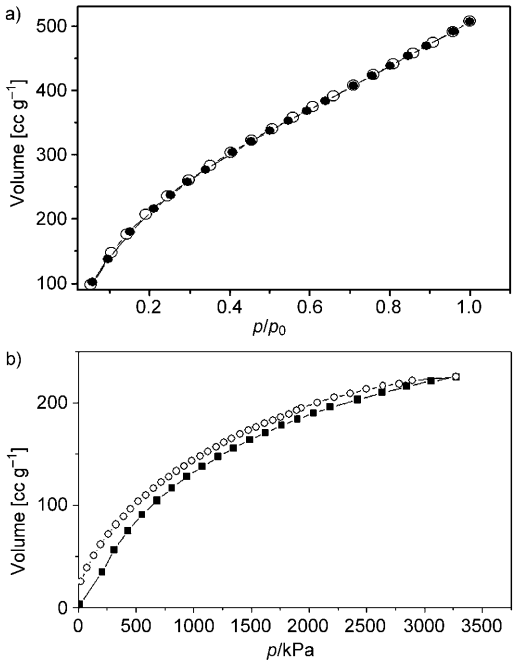

Figure 11. CO_2 adsorption–desorption isotherms of BCN at a) 195 K and 1 atm (○: adsorption, ●: desorption), b) RT and 30 bar (■: adsorption, ○: desorption).

Theoretical calculations: The structure of BCN (atomic positions as well as the periodicity of the supercell) was relaxed to the minimum energy for various chemical orderings (Figure 12). The lattice constants of the six configurations vary within one percent of each other and are the smallest (7.52 Å) for the lowest-energy configuration (vi). Substitution of B and N for two thirds of carbon atoms results in an expansion of the graphene lattice by about 1.5 to 2 percent. In Figure 13 we show the energies of the different configurations as a function of the periodic cell. The cohesive energy of the lowest-energy configuration (vi) is 8.61 eV/atom, which is smaller than that of graphene (9.16 eV/atom) and BC_4N (8.93 eV/atom).[4,16] In this structure, we notice the presence of interlinked local structural motifs of BN_3 and NB_3, similar to those known to be responsible for the stability of BC_4N. In contrast to BC_4N, in which the elastic modulus was estimated to be higher than that of graphene for some of the higher-energy configurations,[4] the modulus of BCN (Table 1) is consistently smaller than that of graphene. We see from the electronic density of states in Figure 14 that two of the higher-energy configurations of BCN are metallic. The lowest-energy configuration has a band gap of about 1.8 eV.

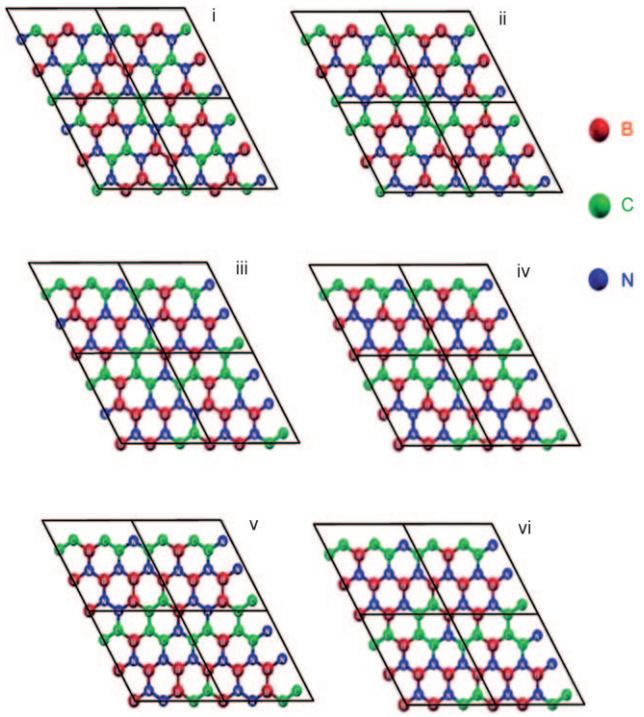

Figure 12. Different chemical ordering of B and N on the graphene lattice.

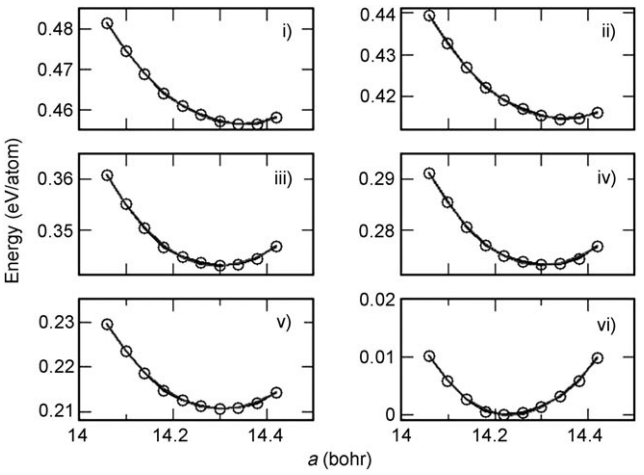

Figure 13. Energetics of different configurations of BCN as a function of the size of the periodic cell.

Table 1. Lattice constant, bulk modulus and cohesive energy of BCN with different ordering of B and N on graphene lattice.

Structure of BCN [a]	Lattice constant [Å]	Bulk modulus [Pa m]	E_{coh} [eV/atom]
i	7.59	159	8.15
ii	7.59	150	8.19
iii	7.57	165	8.27
iv	7.57	157	8.34
v	7.57	158	8.40
vi	7.52	174	8.61

[a] See Figure 12.

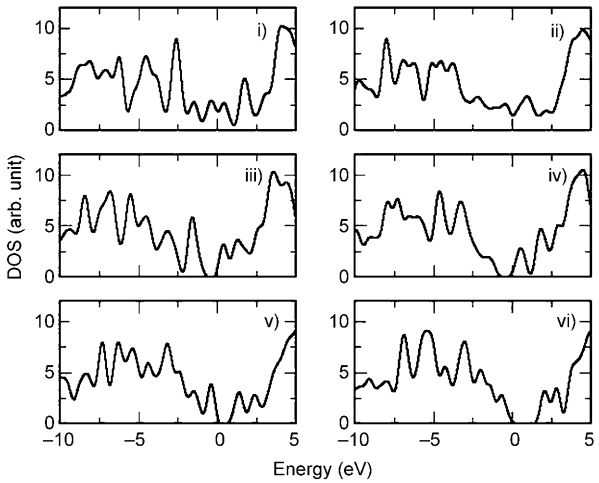

Figure 14. Electronic density of states of BCN with different ordering of B, C and N.

Our theoretical analysis of the stability of graphene-like structures of BC_4N[15,16] and BCN shows that NB_3 and BN_3 local motifs are energetically favourable, which results in the coexistence of C- and BN-rich regions in both BCN and BC_4N. The interface between these regions is essentially a curve (or a line) that behaves electronically similar to the edges of graphene nano-ribbons or -flakes. Such an interface with structure of a zigzag edge has magnetically polarised edge states,[32] which are coupled antiferromagnetically with those on a nearby edge of similar character. Thus, magnetic properties of BCN and BC_4N are expected to be richer than those of pure graphene, as they arise from 1) edges of the flakes and defects like in graphene,[29] as well as 2) the interfacial edges between BN- and C-rich regions. These two distinct mechanisms are evident in the changes in the slope at two different temperatures ($\approx$225 and 125 K) in the FC and ZFC curves of magnetisation. However, as the coupling between spin-polarised states at neighbouring edges is antiferromagnetic, overall magnetic moments are smaller in BCN. More detailed analysis of magnetic interactions in BCN will be reported elsewhere.

Although there are numerous configurations possible for BCN, we only considered the minimum-energy configuration (vi in Figure 13) of BCN and graphene for examining the CO_2 adsorption. In a supercell with 3×3 unit cells (18 atoms), we placed one, two and three CO_2 molecules about 4 Å away (in the initial structure) from the BCN and graphene sheets, corresponding to 20, 40 and 60 wt% coverages of adsorption, respectively. In each case, we considered various sites of adsorption: 1) sites (B, C and N) and 2) the centre of a hexagonal ring. We also considered different orientations of CO_2 molecules in the initial structure: 1) the axis of the CO_2 molecules perpendicular to the atomic plane and 2) the axis of the CO_2 molecules parallel to the atomic plane, with orientations along different in-plane crystallographic directions. In each case, the structure was relaxed, keeping the periodicity fixed, and the adsorption energy, E_{ads}, was determined from Equation (5):

$$E_{ads} = \{E_{n-CO_2/BCN} - (E_{BCN} + n^* E_{CO_2})\}/n \quad (5)$$

in which n is the number of CO_2 molecules, E_{BCN}, E_{CO2} and $E_{n-CO_2/BCN}$ are the energies of the optimised structures of BCN, an isolated CO_2 molecule, and a supercell with CO_2 on the BCN layer, respectively. A similar procedure was used to examine the adsorption of CO_2 on graphene.

We first learned about the interaction between CO_2 and BCN from studies of adsorption at the lowest coverage (20 wt%, one CO_2 molecule per supercell) in which the effects of interactions between CO_2 molecules and images are weak. We find the following atomic sites in BCN to be strongly adsorbing sites: 1) nitrogen bonded with at least one carbon atom, which is likely have a weak negative charge; 2) boron bonded with three nitrogen atoms, which would attract negatively charged oxygen of the molecule and 3) carbon bonded with two nitrogen atoms, which would develop a slightly positive charge to attract the molecule.

Adsorption of CO_2 at the centre of certain hexagonal rings is found to be stronger than that at the atomic sites. In this case, the molecule prefers to be in a plane parallel to the BCN plane. The rings showing strong adsorption of CO_2 typically have at least two carbon atoms and at least a pair of B and N atoms. Secondly, rings with corner atoms that are weak adsorbing sites usually exhibit strong adsorption at the centre. Among the various orientations of CO_2 molecules lying flat on the ring, the one with the axis along the C–B or C–N diagonal of the ring is energetically more favourable. In the lowest-energy configuration, the energy of adsorption of CO_2 with 20 wt% on BCN is 2.79 kJ mol^{-1}, which corresponds to only 0.7 kJ mol^{-1} for graphene. At this coverage, a CO_2 molecule is about 3.71 Å above the BCN plane and 3.83 Å above the graphene plane.

At a higher coverage of 40 wt% (two CO_2 molecules per supercell used here), interactions between nearby CO_2 molecules become important and an initial configuration with CO_2 molecules in the plane parallel to the atomic planes and on top of a ring centre relax to a structure in which a molecule is adsorbed closer to the atomic sites. Our estimate of the adsorption energy at this coverage on BCN is 3.67 kJ mol^{-1} compared with 1 kJ mol^{-1} on graphene. The spread in the adsorption energies in different configurations is from zero to a couple of kJ mol^{-1} (Figure 15). At an adsorption coverage of 60 wt% ($3\,CO_2$ molecules per supercell), has the highest adsorption energy of 3.73 kJ mol^{-1} on BCN compared to 2.04 kJ mol^{-1} on graphene. In this case, the orientation of CO_2 molecules is mixed, two in plane and one perpendicular to the plane. For a higher coverage of 80 wt% ($4\,CO_2$ per supercell), adsorption is not energetically favourable (Figure 15). This is mostly due to the interaction between CO_2 molecules at small separations. Thus, we find adsorption at all coverages of CO_2 on BCN is stronger than that on graphene. Typically, the distance between the adsorbed CO_2 molecule and the BCN plane is about 3% smaller than that in graphene, reflecting stronger bonding in the former case. Furthermore, the distance of the CO_2 mole-

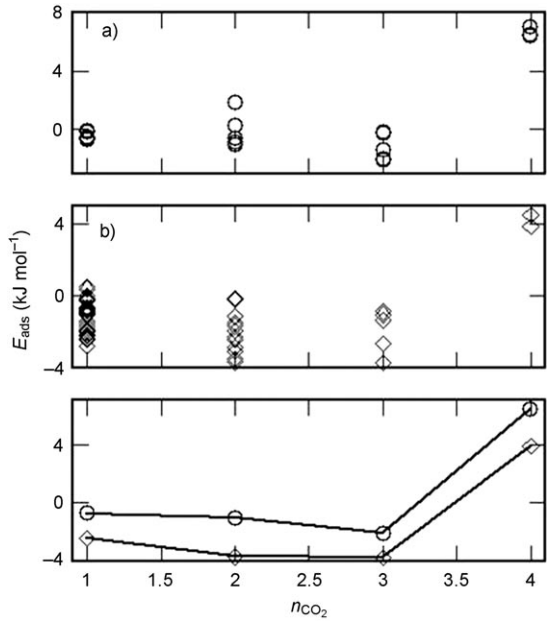

Figure 15. Energies of adsorption of CO_2 molecules at different coverages (n molecules per 18 atom cell) with different configurations of adsorption sites in a) graphene, b) BCN. c) Comparison of energies for the strongest adsorption of CO_2 on graphene (○) and BCN (◇).

cule from the BCN plane is 3.71, 3.74 and 3.89 Å when the coverage is 20, 40 and 60 wt%, respectively.

From the electronic density of states (EDOS) (Figure 16), it is clear that the peaks corresponding to electronic states of adsorbed CO_2 molecules are far from the Fermi energy in both BCN and graphene. They are slightly broad in the case of BCN, becoming even broader and shifted slightly to lower energies with the increasing CO_2 adsorption, reflecting an increased interaction between the molecule and the lattice. After a close examination of the electronic energies, we noticed that a small gap opens up in the case of graphene upon adsorption of CO_2 molecules, whereas the gap in BCN reduces slightly. Visualisation of the electronic states near the gap of BCN reveals a small overlap with molecules, reflecting weak charge transfer between the molecule and the lattice.

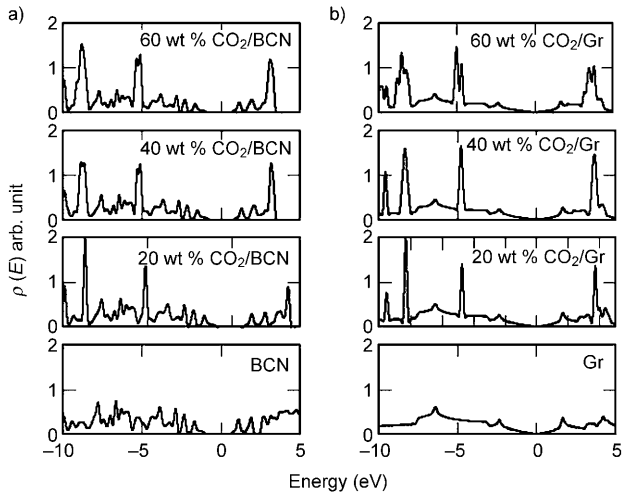

Figure 16. Density of electronic states of the minimum-energy configuration of a) BCN and b) graphene, with CO_2 adsorbed at different wt%.

Conclusion

It has been possible to synthesise a $B_xC_yN_z$ composition with $x=y=z=1$ by reacting high-surface-area activated charcoal with urea and boric acid. It has a two-dimensional layered structure. AFM measurements show that BCN mainly consists of two to three layers, which establishes its resemblance to few-layer graphene.[3] BCN prepared by us is a microporous material exhibiting type I N_2 adsorption–desorption isotherms at 77 K and a very large surface area of 2911 m^2g^{-1}. The extraordinarily high CO_2 uptake of BCN is noteworthy. Theoretical calculations show that the structure is likely to be one with C–C, B–N and C–N bonds. BCN is predicted to be an insulator relative to graphene, as is indeed found experimentally. Adsorption of CO_2 on a single layer of BCN is stronger than that on graphene. Electrostatic interactions between the B and N sites and oxygen atoms of CO_2 and a small overlap between the electronic states of the molecule and lattice govern the interaction between BCN and CO_2. BCN has a finite energy gap and shows the presence of both ferromagnetic and antiferromagnetic features.

Experimental Section

Synthesis: Activated charcoal (1 g, surface area 1256 m^2g^{-1}) was thoroughly mixed with a solution of boric acid (0.3 g) and urea (3.6 g) in water (40 mL). The mixture was warmed at 60 °C to form a thick slippery liquid, which was then dried at the same temperature. The dried mixture was heated in a tube furnace at 900 °C for 10 h in a N_2 atmosphere. After cooling it to room temperature, the sample was heated in an NH_3 environment to 930 °C for 3 h. The black-coloured product obtained after the reaction was then characterised.

Characterisation: The morphology of the product was examined by TEM with a JEOL JEM 3010 instrument (Japan) operated at an accelerating voltage of 300 kV, and field-emission scanning electron microscope (FESEM, FEI Nova-Nano SEM-600, Netherlands). XRD patterns were recorded at room temperature with a Rich-Siefert 3000-TT diffractometer using $Cu_{K\alpha}$ radiation. XPS measurements were carried out using an ESCALAB MKIV spectrometer employing $Al_{K\alpha}$ (1486.6 eV) as photon source. EEL spectra were recorded by using an FEI, TECNAI F30 or TITAN transmission electron microscope equipped with an energy filter for EELS operating at 300 kV. Raman spectra were recorded by using a LabRAM HR with a 633 nm line from a HeNe laser. Thermogravimetric analysis was performed by using a Mettler Toledo Star system. A QUANTACHROME AUTOSORB-1C surface area analyser was used for gas adsorption studies. Surface areas were obtained from nitrogen adsorption–desorption isotherms at 77 K. High-pressure gas sorption isotherm measurements were carried out on a BELSORP-HP, BEL JAPAN high-pressure instrument. Dead volume of the sample cell was measured with He of 99.999% purity. Non-ideal correction for hydrogen gas was done by applying virial coefficients at the respective measurement temperature. The adsorption isotherm of MeOH (at 298 K) was measured in the gaseous state by using a BELSORP-aqua volumetric adsorption instru-

ment from BEL, Japan. DC resistance measurements were carried out by the standard four-probe method using the resistivity option in the Physical Property Measurement System (PPMS), Quantum Design, USA. Magnetic measurements were performed by employing a vibrating sample magnetometer (VSM) in the PPMS. AFM measurements were performed by using a NanoMan instrument.

Methods of calculations: We used plane-wave self-consistent field (PWSCF)[20] implementation of DFT, with a generalised gradient approximation (GGA)[21] to exchange the correlation energy of electrons and ultrasoft pseudopotentials,[22] to represent the interaction between ionic cores and valence electrons. Kohn–Sham wave functions were represented with a plane-wave basis with an energy cutoff of 25 Ry and charge density cutoff of 150 Ry. BCN and graphene were simulated by using 3X3 super cell (chosen to have a coverage of CO_2 that is close to the experimental setup) with periodic boundary conditions and a vacuum of 16 Å in the direction perpendicular to the atomically planar sheets. Integration over the Brillouin zone was sampled with a Monkhorst-Pack scheme[32] with a 5X5X1 mesh of k points and occupation numbers were smeared by using a Methfessel-Paxton scheme[33] with broadening of 0.003 Ry. For each concentration or coverage of CO_2 adsorption, a CO_2 molecule was placed at various possible sites and orientations of the molecule and the structure was relaxed to minimise the energy. For BCN, we considered various configurations of chemical ordering of B and N on graphene and used the lowest-energy configuration in the analysis of CO_2 adsorption.

Acknowledgements

K.R. acknowledges CSIR, India for a fellowship. K.P.S.S.H. is thankful to DRDO, India for financial support.

[1] M. Kawaguchi, *Adv. Mater.* **1997**, *9*, 615.
[2] A. K. Geim, K. S. Novoselov, *Nat. Mater.* **2007**, *6*, 183.
[3] C. N. R. Rao, K. Biswas, K. S. Subrahmanyam, A. Govindaraj, *J. Mater. Chem.* **2009**, *19*, 2457.
[4] L. S. Panchakarla, K. S. Subrahmanyam, S. K. Saha, A. Govindaraj, H. R. Krishnamurthy, U. V. Waghmare, C. N. R. Rao, *Adv. Mater.* **2009**, DOI: 10.1002/adma.200901285.
[5] O. Stephan, P. M. Ajayan, C. Colliex, P. Redlich, J. M. Lambert, P. Bernier, P. Lefin, *Science* **1994**, *266*, 1683.
[6] P. Redlich, J. Loeffler, P. M. Ajayan, J. Bill, F. Aldinger, M. Riihle, *Chem. Phys. Lett.* **1996**, *260*, 465.
[7] K. Suenaga, C. Colliex, N. Demoncy, A. Loiseau, H. Pascard, F. Willaime, *Science* **1997**, *278*, 653.
[8] Y. Zhang, H. Gu, K. Suenaga, S. lijirna, *Chem. Phys. Lett.* **1997**, *279*, 264.
[9] R. Sen, B. C. Satishkumar, A. Govindaraj, K. R. Harikumar, G. Raina, J. P. Zhang, A. K. Cheetham, C. N. R. Rao, *Chem. Phys. Lett.* **1998**, *287*, 671.
[10] W. Q. Han, J. Cumings, X. Huang, K. Bradley, A. Zettl, *Chem. Phys. Lett.* **2001**, *346*, 368.
[11] M. Terrones, D. Golberg, N. Grobert, T. Seeser, M. Reyes-Reyes, M. Mayne, R. Kamalakaran, P. Dorozhkin, Z. C. Dong, H. Terrones, M. Ruhle, Y. Bando, *Adv. Mater.* **2003**, *15*, 1899.
[12] W. L. Wang, X. D. Bai, K. H. Liu, Z. Xu, D. Golberg, Y. Bando, E. G. Wang, *J. Am. Chem. Soc.* **2006**, *128*, 6530.
[13] S. Y. Kim, J. Park, H. Chul Choi, J. P. Ahn, J. Q. Hou, H. S. Kang, *J. Am. Chem. Soc.* **2007**, *129*, 1705.
[14] C. N. R. Rao, A Govindaraj, *Adv. Mater.* **2009**, *21*, 4208.
[15] K. Raidongia, D. Jagadeesan, M. U. Kahaly, U. V. Waghmare, S. K. Pati, M. Eswaramoorthy, C. N. R. Rao, *J. Mater. Chem.* **2008**, *18*, 83.
[16] K. Raidongia, K. P. S. S. Hembram, U. V. Waghmare, M. Eswaramoorthy, C. N. R. Rao, unpublished results.
[17] R. B. Kaner, J. Kouvetakis, C. E. Warble, M. L. Sattler, N. Bartlett, *Mater. Res. Bull.* **1987**, *22*, 399.
[18] A. Vinu, M. Terrones, D. Golberg, S. Hishita, K. Ariga, T. Mori, *Chem. Mater.* **2005**, *17*, 5887.
[19] a) A. Gomathi, A. Sundaresan, C. N. R. Rao, *J. Solid State Chem.* **2007**, *180*, 291; b) A. Gomathi, S. Reshma, C. N. R. Rao, *J. Solid State Chem.* **2009**, *182*, 72.
[20] S. Baroni, A. D. Corso, S. de Gironcoli, P. Gianozzi, http://www.pwscf.org.
[21] J. P. Perdew, K. Burke, M. Ernzerhof, *Phys. Rev. Lett.* **1996**, *77*, 3865.
[22] D. Vanderbilt, *Phys. Rev. B* **1990**, *41*, 7892.
[23] G. Wang, J. Yang, J. Park, X. Gou, B. Wang, H. Liu, J. Yao, *J. Phys. Chem. C* **2008**, *112*, 8192.
[24] F. Zhuge, S. Yamanaka, *J. Alloys and Compd.* **2008**, *466*, 299.
[25] M. Hubacek, T. Sato, *J. Solid State Chem.* **1995**, *114*, 258.
[26] C. Y. Zhi, X. D. Bai, E. G. Wang, *Appl. Phys. Lett.* **2002**, *80*, 3590.
[27] J. Wu, W. Q. Han, W. Walukiewicz, J. W. Ager III, W. Shan, *Nano Lett.* **2004**, *4*, 647.
[28] K. S. Subrahmanyam, L. S. Panchakarla, A. Govindaraj, C. N. R. Rao, *J. Phys. Chem. C* **2009**, *113*, 4257.
[29] H. S. S. R. Matte, K. S. Subrahmanyam, C. N. R. Rao, *J. Phys. Chem. C* **2009**, *113*, 9982.
[30] K. S. W. Sing, D. H. Everett, R. A. Haul, L. Moscou, R. A. Pierotti, J. Rouquerol, T. Siemieniewska, *Pure Appl. Chem.* **1985**, *57*, 603.
[31] A. Ghosh, K. S. Subrahmanyam, K. Saikrishna, S. Datta, A. Govindaraj, S. K. Pati, C. N. R. Rao, *J. Phys. Chem. C* **2008**, *112*, 15704.
[32] Y. W Son, M. L. Cohen, S. G. Louie, *Nature* **2006**, *444*, 347.
[33] H. J. Monkhorst, J. D. Pack, *Phys. Rev. B* **1976**, *13*, 5188.
[34] M. Methfessel, A. Paxton, *Phys. Rev. B* **1989**, *40*, 3616.

Received: September 8, 2009
Published online: November 27, 2009

